

# Spatial transcriptomics unveils ZBTB11 as a regulator of cardiomyocyte degeneration in arrhythmogenic cardiomyopathy

Cornelis J. Boogerd <sup>1†</sup>, Grégory P.A. Lacraz <sup>1†</sup>, Ábel Vértesy <sup>1,2†</sup>,  
Sebastian J. van Kampen <sup>1</sup>, Ilaria Perini<sup>1</sup>, Hesther de Ruiter<sup>1</sup>, Danielle Versteeg<sup>1</sup>,  
Andreas Brodehl <sup>3</sup>, Petra van der Kraak<sup>4</sup>, Mauro Giacca <sup>5</sup>, Nicolaas de Jonge<sup>6</sup>,  
Jan Philipp Junker<sup>7</sup>, Alexander van Oudenaarden <sup>1</sup>, Aryan Vink <sup>4†</sup>,  
and Eva van Rooij <sup>1,6\*†</sup>

<sup>1</sup>Hubrecht Institute, Royal Netherlands Academy of Arts and Sciences (KNAW) and University Medical Center Utrecht, Utrecht, The Netherlands; <sup>2</sup>Institute of Molecular Biotechnology of the Austrian Academy of Sciences (IMBA), Vienna, Austria; <sup>3</sup>Heart and Diabetes Center NRW, University Hospital of the Ruhr-University Bochum, Bad Oeynhausen, Germany; <sup>4</sup>Department of Pathology, University Medical Center Utrecht, Utrecht University, Utrecht, The Netherlands; <sup>5</sup>School of Cardiovascular Medicine and Sciences, King's College London British Heart Foundation Centre, London, UK; <sup>6</sup>Department of Cardiology, University Medical Center Utrecht, Utrecht University, Utrecht, The Netherlands; and <sup>7</sup>Berlin Institute for Medical Systems Biology, Max Delbrück Center for Molecular Medicine, Berlin, Germany

Received 6 July 2021; revised 12 April 2022; accepted 20 April 2022; online publish-ahead-of-print 16 May 2022

Time of primary review: 29 days

## Aims

Arrhythmogenic cardiomyopathy (ACM) is an inherited cardiac disorder that is characterized by progressive loss of myocardium that is replaced by fibro-fatty cells, arrhythmias, and sudden cardiac death. While myocardial degeneration and fibro-fatty replacement occur in specific locations, the underlying molecular changes remain poorly characterized. Here, we aim to delineate local changes in gene expression to identify new genes and pathways that are relevant for specific remodelling processes occurring during ACM.

## Methods and results

Using Tomo-Seq, genome-wide transcriptional profiling with high spatial resolution, we created transmural epicardial-to-endocardial gene expression atlases of explanted ACM hearts to gain molecular insights into disease-driving processes. This enabled us to link gene expression profiles to the different regional remodelling responses and allowed us to identify genes that are potentially relevant for disease progression. In doing so, we identified distinct gene expression profiles marking regions of cardiomyocyte degeneration and fibro-fatty remodelling and revealed Zinc finger and BTB domain-containing protein 11 (*ZBTB11*) to be specifically enriched at sites of active fibro-fatty replacement of myocardium. Immunohistochemistry indicated *ZBTB11* to be induced in cardiomyocytes flanking fibro-fatty areas, which could be confirmed in multiple cardiomyopathy patients. Forced overexpression of *ZBTB11* induced autophagy and cell death-related gene programmes in human cardiomyocytes, leading to increased apoptosis.

## Conclusion

Our study shows the power of Tomo-Seq to unveil new molecular mechanisms in human cardiomyopathy and uncovers *ZBTB11* as a novel driver of cardiomyocyte loss.

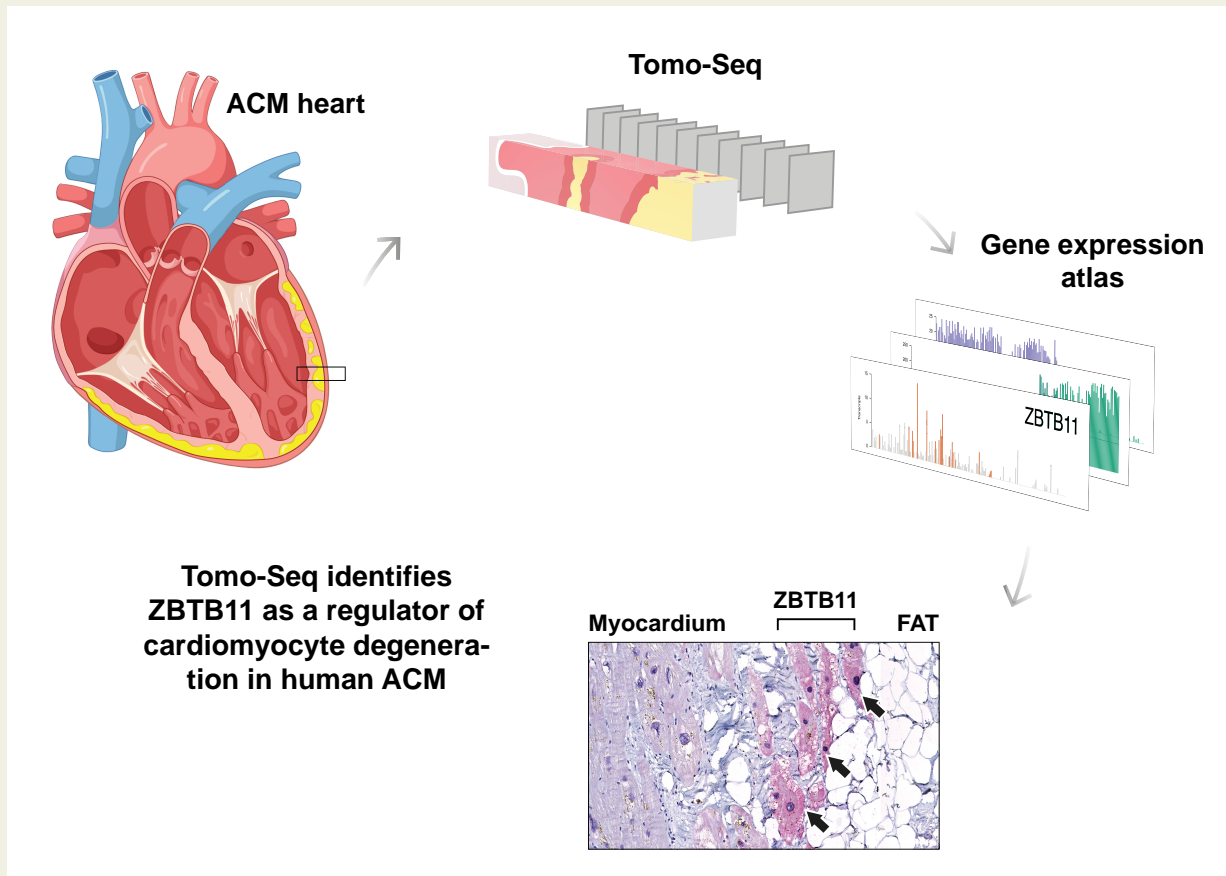
\* Corresponding author. E-mail: [e.vanrooij@hubrecht.eu](mailto:e.vanrooij@hubrecht.eu)

† These authors contributed equally to this work.

© The Author(s) 2022. Published by Oxford University Press on behalf of the European Society of Cardiology.

This is an Open Access article distributed under the terms of the Creative Commons Attribution-NonCommercial License (<https://creativecommons.org/licenses/by-nc/4.0/>), which permits non-commercial re-use, distribution, and reproduction in any medium, provided the original work is properly cited. For commercial re-use, please contact [journals.permissions@oup.com](mailto:journals.permissions@oup.com)

## Graphical Abstract



Using spatial transcriptomics, transmural epicardial-to-endocardial gene expression atlases of human ACM hearts were generated. Linking gene expression profiles to regional remodelling responses revealed Zinc finger and BTB domain-containing protein 11 (ZBTB11) to be specifically enriched at sites of active fibro-fatty replacement of myocardium. Immunohistochemistry indicated ZBTB11 to be induced in cardiomyocytes flanking fibro-fatty areas, which could be confirmed in multiple cardiomyopathy patients. This study shows the power of Tomo-Seq to unveil new molecular mechanisms in human cardiomyopathy and uncovers ZBTB11 as a novel driver of cardiomyocyte loss.

**Keywords** Tomo-Seq • Arrhythmogenic cardiomyopathy • Cardiomyocyte degeneration • ZBTB11

## 1. Introduction

Arrhythmogenic cardiomyopathy (ACM) is a hereditary heart disease characterized by progressive fibro-fatty replacement of the myocardium, ventricular arrhythmias, and progressive ventricular dysfunction.<sup>1</sup> While relatively rare (prevalence 1/2500–1/5000), ACM is an important cause of sudden cardiac death in young individuals and athletes.<sup>2</sup> ACM is broadly considered a desmosomal disease as most pathogenic variants are found in genes encoding components of the cardiac desmosome.<sup>3</sup> Cardiac desmosomes are adhesion junctions composed of cadherins, armadillo proteins, and plakins that provide mechanical connections between cardiomyocytes and their intermediate filament system.<sup>4</sup> In most ACM populations, heterozygous variants in *PKP2*, encoding plakophilin-2, result in premature termination codons or abnormal splicing.<sup>5,6</sup> Current therapies for ACM are designed to prevent ventricular arrhythmias and sudden death and have been focused on managing the disease, but are unable to halt the progression of ACM.<sup>7</sup> As such, there is ample opportunity to improve medical treatment of patients suffering from ACM.

In ACM, viable myocardium is replaced by fibrous and fatty tissue due to cumulative loss of cardiomyocytes.<sup>8</sup> These pathological hallmarks of the disease are usually distinctly present at the epicardial surface, but islands of degenerating cardiomyocytes surrounded by fibro-fatty patches can also be found throughout the septal and left ventricular myocardial tissue. Morphologically, these cardiomyocytes show features of myofibrillar loss and hyperchromatic changes in nuclear morphology that can eventually lead to cardiomyocyte death.<sup>8</sup> Functionally, the progressive loss of myocardium may cause intraventricular conduction delay and re-entry circuits triggering ventricular arrhythmias. A better understanding of the molecular mechanisms driving this aspect of pathological remodelling could aid in the development of enhanced therapeutic strategies.

While genome-wide transcriptome analysis on extracts from diseased tissues has been instrumental in improving our understanding of the gene regulatory networks involved in disease, this information often came with little or no spatial information. Tomo-Seq allows for the addition of spatial information to sequencing data by analysing the transcriptome of microdissected tissue.<sup>9,10</sup> Using this technology on the

infarcted mouse heart, our group recently identified SOX9 as a key regulator of cardiac fibrosis.<sup>11</sup> Here, we combined Tomo-Seq on human ACM hearts with classical histological approaches to determine gene expression changes underlying disease-driving mechanisms in ACM. Epicardial-to-endocardial Tomo-Seq of explanted ACM hearts from *PKP2* and *DSP* mutation carriers revealed gene expression profiles specific for the different regional remodelling responses and allowed us to identify the transcription factor *ZBTB11* to function as a potent inducer of cardiomyocyte atrophy. These data show the power of using Tomo-Seq to unveil molecular mechanisms driving local remodelling responses and uncover *ZBTB11* as a potential new target for cardiomyopathy. Our gene expression atlases of the human ACM heart could serve as a reference for future studies, providing novel inroads to study disease mechanisms and for the development of therapeutic approaches.

## 2. Methods

### 2.1 Study design

The overall objective of the study was to identify new genes and pathways that are relevant for specific remodelling processes occurring during ACM. We obtained explanted hearts from five ACM patients with desmosomal gene mutations and hearts from three patients with DCM. ACM hearts were selected based on histological parameters such as the presence of fibro-fatty replacement tissue in right ventricular (RV) and left ventricular (LV) free walls. We performed Tomo-Seq on two human ACM hearts with mutations in *PKP2* and *DSP* to discover local clusters of gene expression. The inclusion of sections for analysis was based on read counts and quality checks as previously described and detailed in [Supplementary material online, Methods](#).<sup>9</sup> Tomo-Seq results were validated by immunostaining in the additional hearts.

*ZBTB11* protein function in cardiomyocytes was assessed by overexpressing *ZBTB11* in iPS-CM using AAV6. We performed RNA-Seq on these cells to obtain transcriptome-wide differential gene expression profiles induced by *ZBTB11*. Gene set enrichment analysis (GSEA) was performed to identify the pathways that were most significantly affected by *ZBTB11* overexpression, to identify the biological roles of *ZBTB11* in cardiomyocytes.

### 2.2 Human tissue

Collection of the human heart tissue was approved by the scientific advisory board of the biobank of the University Medical Center Utrecht, Utrecht, The Netherlands (protocol no. 12/387) and conformed to the principles outlined in the Declaration of Helsinki. Human hearts were collected during heart transplantation and frozen for Tomo-Seq analysis or fixed in formalin and embedded in paraffin for histology and immunohistochemistry. The *PKP2* mutation, c.2412G > A (p.Trp804X, NM\_001005242.2) was previously annotated *PKP2* c. 2544G > A (p.Trp848X), according to the coordinates of *PKP2* isoform 2b (NM\_004572.4), which is less abundant in the heart.<sup>12</sup>

### 2.3 Tomo-Seq on *PKP2* p.Trp804X ACM heart

Detailed description of Tomo-Seq methods and data analysis is provided in [Supplementary material online, Methods](#). Briefly, 3/3 mm width/height portions of cardiac human tissue spanning from the epicardium towards the endocardium of the LV lateral wall were cryosectioned at 100  $\mu$ m thickness as described.<sup>9</sup> RNA was extracted and samples were subjected to paired-end sequencing at 50 bp read length on an Illumina HiSeq

2500. Two hundred and fourteen high-quality sections with >1000 transcripts, with 1391 genes expressed above 5 unique transcripts in at least 3 sections were retained for further analysis. We calculated the pairwise Spearman correlation of sections and performed hierarchical clustering with complete linkage. RNA-Seq data are deposited on Gene Expression Omnibus, accession number GSE114770, and analysis scripts are available under: <https://github.com/vertesy/ACM.Tomo-Seq>.

### 2.4 Differentiation and transduction of iPS-derived cardiomyocytes

To obtain human cardiomyocytes, we used human-induced pluripotent stem cells (LUMC0099iCTRL04 generated by the LUMC hIPS Core facility) and differentiated to cardiomyocytes (iPS-CM) as described previously.<sup>13</sup> iPS-CM were seeded at 0.2 million cells/cm<sup>2</sup> and transduced with AAV6-GFP or AAV6-*ZBTB11* at 5000 viral genomes per cell. The medium was changed 3 days after transduction, and cells were harvested for protein or RNA extraction 4 or 7 days after transduction.

### 2.5 RNA-Seq

Total RNA was extracted using the standard TRIzol (Invitrogen) protocol and used for library preparation and sequencing. Deseq2<sup>14</sup> was used to identify differentially expressed genes, using the Benjamini and Hochberg adjusted *P*-value of 0.05 and fold change of 1.5 as thresholds.

### 2.6 Statistical analysis

Values are presented as mean  $\pm$  standard error of the mean. Statistical analyses were performed using a two-tailed unpaired Student's *t*-test or one-way analysis of variance as indicated in results or figure legends using Prism 6 (GraphPad Software, Inc.). Pearson's correlation coefficients were used to calculate gene pair correlation based on gene expression in human samples. KEGG pathways are ranked by their respective *P*-value corrected for multiple hypotheses testing using the Benjamini-Hochberg method. A *P*-value of <0.05 was considered statistically significant.

## 3. Results

### 3.1 Cardiac remodelling due to a pathogenic nonsense mutation in *PKP2*

To start exploring molecular mechanisms underlying ACM, we obtained an explanted heart of a male patient with a known pathogenic nonsense *PKP2* mutation, c.2412G > A (p.Trp804X, NM\_001005242.2).<sup>12</sup> Gross examination of the explanted heart revealed cardiomyocyte degeneration and severe fibro-fatty replacement of both ventricular walls, with an almost complete absence of viable myocardium in the RV free wall (*Figure 1A* and *B*). Histological examination of both RV and LV<sup>15</sup> of the ACM heart (*PKP2*-mut) indicated complete subepicardial fibro-fatty replacement (Fibro-fatty region), patches of degenerating cardiomyocytes flanked by fibro-fatty tissue (Composite region), and areas composed of mainly cardiomyocytes (Myocardial region; *Figure 1B* and *C*, and see [Supplementary material online, Figure S1A](#)). The fibro-fatty replacement was undetectable in non-failing control tissue (NF control). Sanger sequencing of the explanted ACM heart and tissue from a healthy control donor heart validated the presence of a G to A mutation in the *PKP2* locus at base position 2412 (Codon 804) in the patient-derived sample (*Figure 1D*). The G to A substitution causes a premature stop codon within exon 12. Western blot analysis showed that this mutation resulted in a loss of total *PKP2* compared with NF control (*Figure 1E*

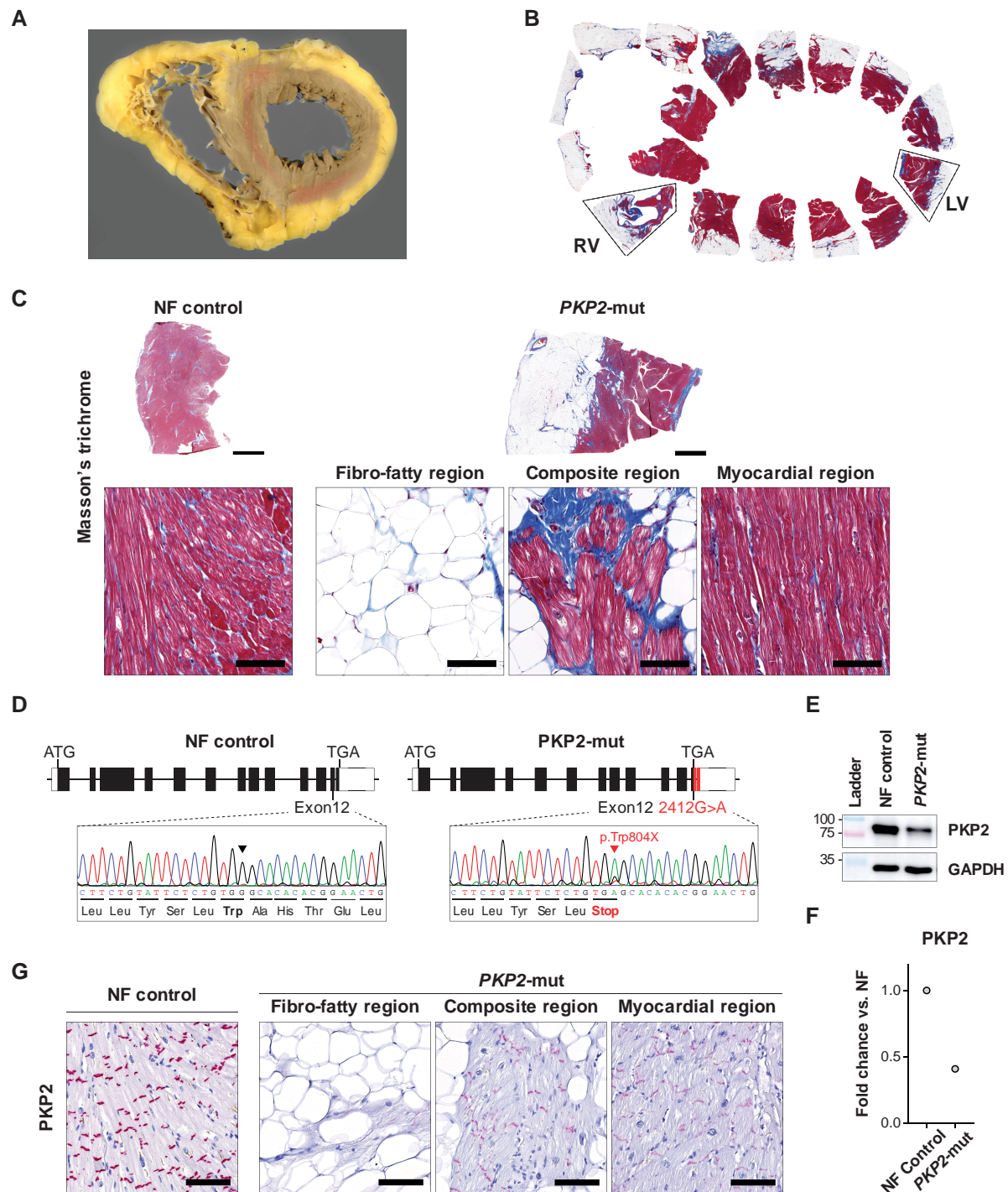


**Figure 1** Mutant *PKP2* heart showing classical signs of ACM remodelling. (A) Ventricular cross-section of the explanted ACM heart from a patient harbouring a *plakophilin-2* mutation (*PKP2*) showing severe biventricular remodelling. (B) Histological overview of the explanted heart stained for Masson's trichrome. LV, left ventricle; RV, right ventricle. Dashed lines mark the LV and RV blocks used in this study. (C) Masson's trichrome staining on transverse LV sections of the ACM heart and NF control heart. Epicardial fibro-fatty, composite (composed of both fibro-fatty cells and myocytes), and myocardial regions are depicted. Scale bars, 5 mm (top) and 100  $\mu$ m (bottom). (D) Sanger sequencing of *PKP2* exon 12 depicting the mutation that introduces a premature termination codon. (E) Western blot analysis of *PKP2* in the control and ACM heart. (F) Quantification of western blot analysis of *PKP2* in the control and ACM heart. (G) *PKP2* immunostaining illustrating reduced *PKP2* levels in patient cardiomyocytes. Scale bars 100  $\mu$ m.

and F), which was confirmed by immunohistochemistry (IHC) for *PKP2*. While *PKP2* was undetectable in the fibro-fatty region, we observed a strongly reduced and less organized *PKP2* signal in the composite and

myocardial regions in the ACM heart in both the LV and the RV compared with NF control (Figure 1G, and see [Supplementary material online, Figure S1B](#)).

## 3.2 Desmosomal and cell junction de-arrangement in response to mutant PKP2

Cardiac desmosomes consist of transmembrane desmosomal cadherins Desmoglein-2 (DSG2) and Desmocollin-2 (DSC2) that bind to the armadillo family proteins Plakoglobin (PKG) and PKP2 which anchor to the plakin family member Desmoplakin (DSP).<sup>16</sup> Since there are data to support molecular crosstalk between PKP2 and other desmosomal genes,<sup>17</sup> we determined their expression in both LV and RV tissue from the explanted heart. IHC indicated a reduction for DSC2 and PKG compared with control which was most pronounced in the RV portion of the explanted ACM heart (see [Supplementary material online, Figure S2A](#)). This was mirrored by a lowering and intracellular redistribution of Connexin43 (Gap junction protein alpha 1; GJA1) in the composite region, where cardiomyocytes are flanked by fibro-fatty cells (see [Supplementary material online, Figure S2B](#)). N-Cadherin (NCAD) is an integral component of adherens junctions residing at the intercalated disk and functions to mechanically and electrically couple adjacent cardiomyocytes. Double staining for dystrophin (DMD, marking cell membranes) and NCAD indicated a marked dyslocalization of NCAD in the areas composed of cardiomyocytes and fibro-fatty cells (Composite region) (see [Supplementary material online, Figure S2C](#)). Western blot analysis indicated that desmosomal proteins DSP and PKG were indeed reduced in the explanted ACM heart compared with NF control hearts (see [Supplementary material online, Figure S1C and D](#)). Notably, NCAD levels were not reduced, indicating that altered NCAD staining in the composite region reflects mis-organization of diseased cardiomyocytes.

Together, these results indicate that the mutation in *PKP2* leads to severe biventricular fibro-fatty remodelling, local cardiomyocyte degeneration in fibro-fatty areas, and dyslocalization or loss of desmosomal and junctional components between cardiomyocytes.

## 3.3 Transmural gene expression analysis of the ACM heart

To link local remodelling responses to precise spatial gene expression changes, we performed Tomo-Seq on the ACM heart. To this end, we microdissected LV free wall tissue and sectioned it at 100  $\mu\text{m}$  resolution going from the epicardium towards the myocardial region of the cardiac wall ([Figure 2A](#)). Sections were subsequently subjected to RNA-Seq, and after quality control (see [Supplementary material online, Figure S3](#)) generated a genome-wide expression atlas across the diseased human ACM heart at a high spatial resolution ([Supplementary material online, data file S1](#)).

In performing a pairwise comparison of sections across all expressed genes, we observed a spatial partitioning, likely reflecting the fibro-fatty region and the myocardial region ([Figure 2B](#)). This was confirmed when looking at the relative expression of well-known marker genes for adipocytes: Perilipin-1 (*PLIN1*); interstitial cells including fibroblasts and smooth muscle cells: Alpha-actin-2 (*ATCA2*); and cardiomyocytes: Desmin (*DES*, [Figure 2C](#)). *PLIN1* peaked mostly in the fatty area located close to the epicardium, while *ACTA2* appeared highly expressed towards the outer epicardial area but also extended into the myocardial portion. *DES* peaked mostly in the myocardial region with some expression in the fatty area. Since Tomo-Seq provides spatial information on gene expression, it allows for correlation analysis between different genes to identify genes with a comparable spatial distribution in transcriptional regulation. Using Z-score transformed traces, we looked for genes with a similar expression pattern as *PLIN1*, *ACTA2*, or *DES*, and noticed the presence of other well-

known genes related to adipocytes, fibroblasts, or cardiomyocytes, like Fatty acid-binding protein 4 (*FABP4*), Collagen type XIV alpha 1 chain (*COL14A1*), and Troponin T2 (*TNNT2*), respectively. However, also genes that are currently unknown to be related to adipocyte, fibroblast, or cardiomyocyte biology could now be linked to *PLIN1*, *ACTA2*, or *DES* ([Figure 2C and D](#), and [Supplementary material online, data file S2](#)). Analysis of the top 150 most similarly regulated genes to *PLIN1*, *ACTA2*, or *DES* revealed functional annotations linked to the known function of the reference genes, such as 'Regulation of lipolysis in adipocytes', 'Focal adhesion', and 'Cardiac muscle contraction', respectively ([Figure 2E](#)).

Together, these data suggest that correlation analysis of Tomo-Seq data can serve to identify new genes and biological functions related to their reference genes.

## 3.4 Local gene expression profiles within the ACM heart

To distinguish types of gene expression profiles, we performed hierarchical clustering of all sections using Pearson's correlation coefficients. We next grouped the sections by similarity on the y-axis and kept the physical epi-to-endocardium order along the x-axis intact ([Figure 3A](#)). Our clustering analysis could bioinformatically segregate three types of sections (indicated as Clusters 1–3). Cluster 1 sections could only be detected at the epicardial, fibro-fatty region of the ACM heart (green,  $n = 76$ ), while two distinct clusters were detected within the myocardial region [annotated Cluster 2, orange ( $n = 29$ ) and Cluster 3, violet ( $n = 109$ )]. Cluster 2 sections were found to be located at the border zone region between the fatty region and myocardial area and interspersed with Cluster 3 sections ([Figure 3A and B](#)).

In looking at the number of reads per section along the sectioning axis, we observed on average a lower read count in the sections from Cluster 1 and the highest read count in sections from Cluster 3 ([Figure 3B](#)). The balance between energy dissipation and storage in tissues is dictated by mitochondrial metabolism in the cell. In plotting the fraction of mitochondrial transcripts (chr M) with all reads along the sectioning axis, we showed these two metrics to be highly correlated and predictive of the cluster the section belonged to, with Cluster 2 sections being in between Cluster 1 and 3 sections ([Figure 3C](#), Pearson's  $r = 0.868$ ). Also, when the sections were projected on the principal component analysis (PCA) map, we found Cluster 1 to segregate from the sections in Clusters 2 and 3, with Cluster 2 sections forming an intermediary between Clusters 1 and 3 ([Figure 3D](#)).

These data indicated that the sections of the ACM heart can be clustered based on different gene expression profiles and that a subset of sections harbours both transcriptional characteristics of the adipogenic and the myocardial areas.

## 3.5 Marker gene expression indicates section identity in the ACM heart

To explore the cellular composition of the individual sections, we used the PCA map generated in [Figure 3D](#) and examined the expression level of key marker genes on a single-section level and validated their expression in the explanted heart ([Figure 4](#)). When projected onto the PCA map, the relative expression of adipocyte markers such as *PLIN1*, *FABP4*, Patatin-like phospholipase domain-containing protein 2 (*PNPLA2*), and Cell death activator CIDE-3 (*CIDEA*) was higher in Cluster 1 sections and extending into Cluster 2 sections ([Figure 4A](#)). By IHC, we could indeed confirm the expression of *PLIN1* and *FABP4* to predominantly mark fat cells ([Figure 4B](#)).

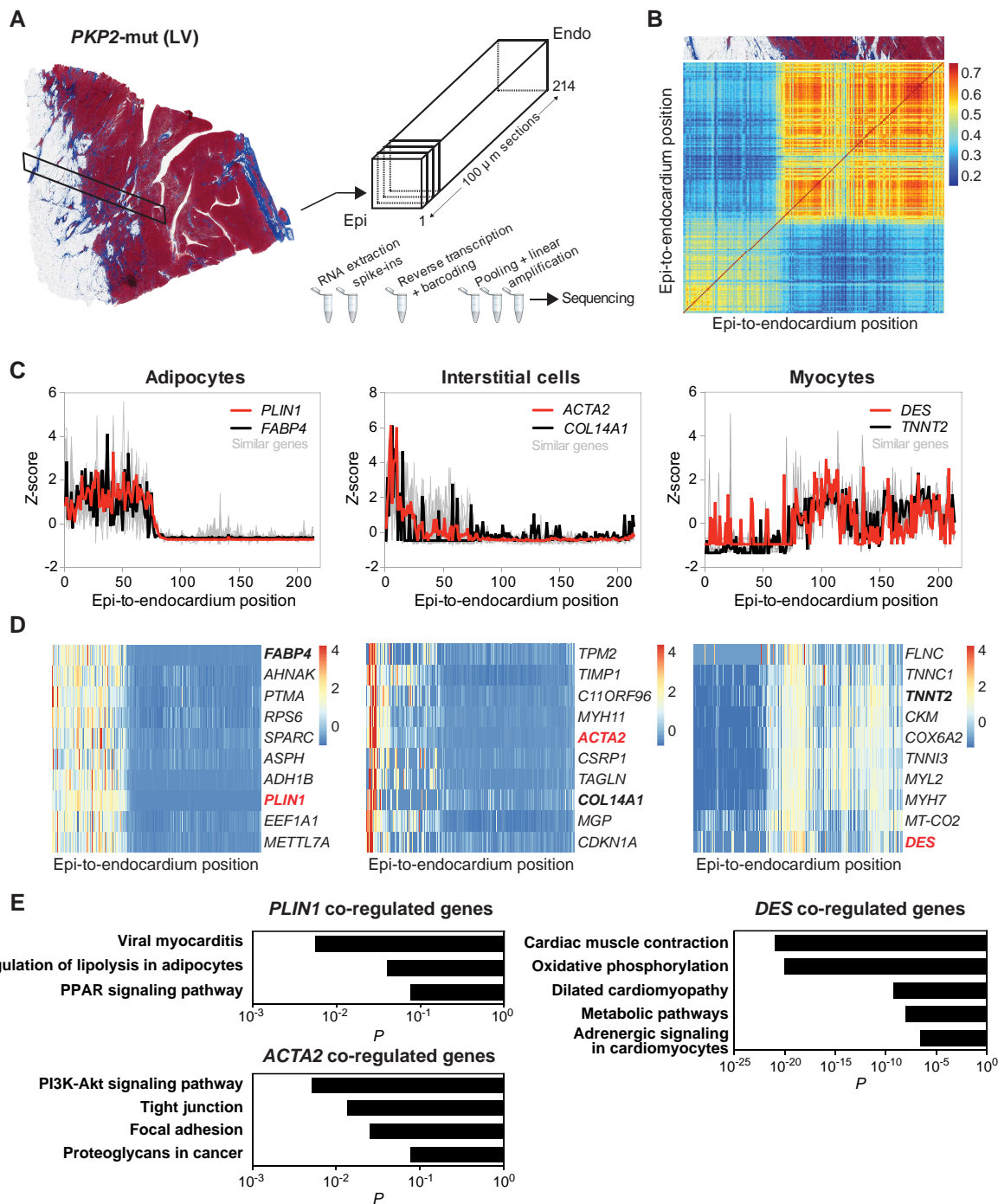


**Figure 2** Transmural gene expression atlas by Tomo-Seq allows the identification of spatially co-expressed genes in the ACM heart. (A) Schematic representation of the Tomo-Seq procedure in the ACM heart. (B) Pairwise correlation for all 214 sections across all expressed genes showing a separation between the epicardial fibro-fatty region (bottom left cluster) and the rest of the myocardium (top right cluster). (C) Z-score normalized spatial expression profiles of top co-regulated genes in the ACM heart. Reference genes for adipocytes, interstitial cells, and cardiomyocytes are shown in red (*PLIN1*, *ACTA2*, and *DES*, respectively), and the 10 most similar genes are shown in black/grey. Similar genes were identified by the smallest Euclidean distance to the respective marker gene. Black bold traces show other known markers for adipocytes, interstitial cells, and cardiomyocytes (*FABP4*, *COL14A1*, and *TNNT2*, respectively). (D) Heatmaps of the top 10 co-regulated genes. (E) Functional annotation of the top 150 similarly regulated genes as either *PLIN1*, *ACTA2*, or *DES*.

While some interstitial cell markers *ACTA2* and Vimentin (*VIM*) were more enriched in the adipogenic sections from Cluster 1, a broader distribution extending towards the Cluster 2 sections was found for other fibroblasts markers like Collagen Type I alpha 2 chain (*COL1A2*) and

Fibronectin (*FN1*) (Figure 4C). IHC for  $\alpha$ SMA showed enrichment in fibro-fatty areas, while *VIM* appeared to be expressed in adipocytes, fibroblasts, and smooth muscle cells (Figure 4D). The cardiomyocyte markers *DES*, Alpha actinin 2 (*ACTN2*), Titin (*TTN*), and skeletal muscle

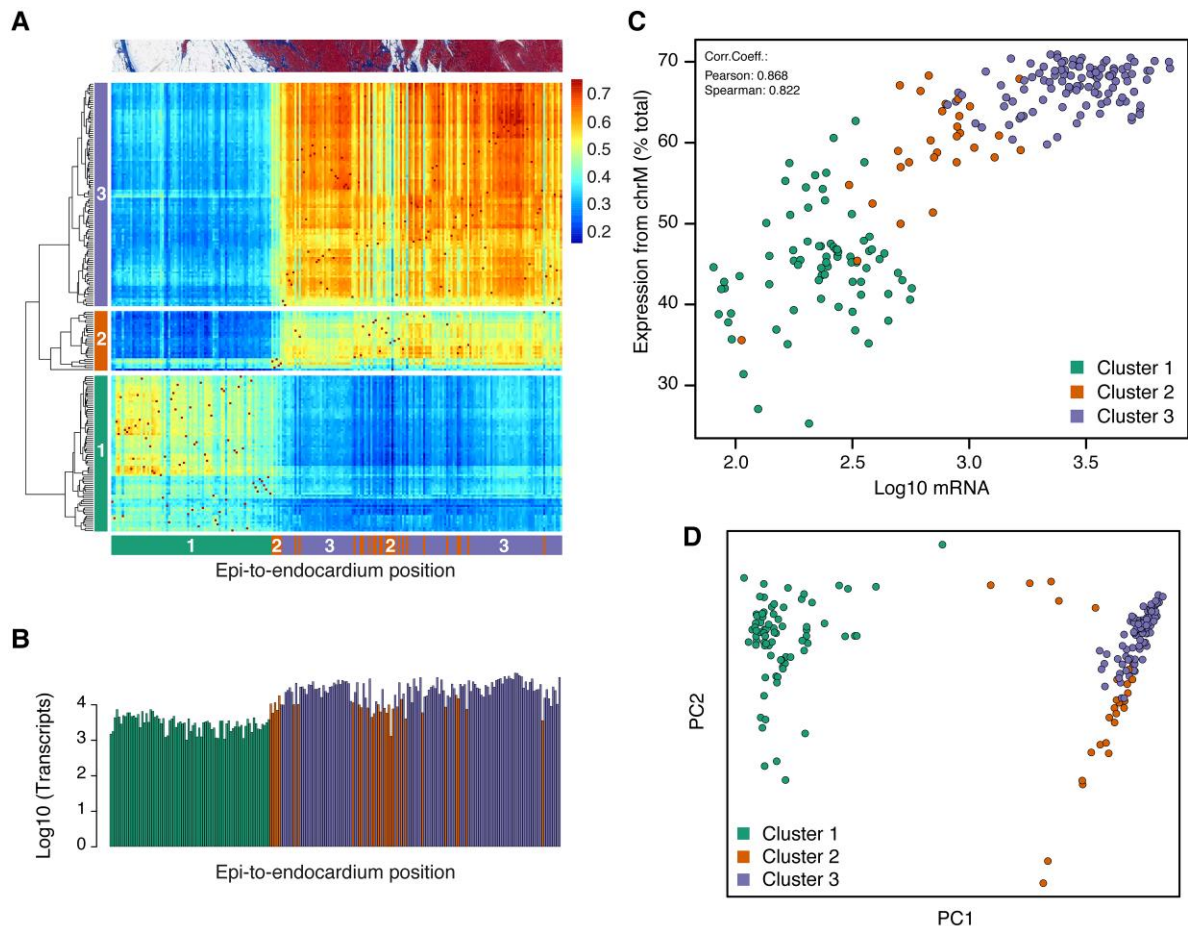


**Figure 3** Semi-supervised clustering identifies sections with distinct gene expression profiles. (A) Pairwise Pearson's correlation of all sections shows heterogeneity within the myocardium. Sections are displayed in epi-to-endocardium order on the x-axis and hierarchically clustered on the y-axis (top three clusters are colour-coded). (B) Transcript counts per section displayed in the same physical order as in A (x-axis). Sections are colour-coded by the three clusters identified in A. (C) Fraction of mitochondrial reads (chr M) vs. the total mRNA content of the sections. Correlation coefficient,  $r = 0.868$  (Pearson);  $r = 0.822$  (Spearman). Each dot is one section colour-coded as in B. (D) PCA plot of all sections with the previously determined cluster identity overlaid in colours (as in B).

alpha actin 1 (*ACTA1*) showed enrichment in the sections coming from Cluster 3 (Figure 4E), which was confirmed by IHC for DES and ACTN2 (Figure 4F).

### 3.6 Cardiomyocyte degeneration gene programme activated in composite sections

To examine the gene expression differences in the different types of sections, we performed pairwise differential gene expression analysis between the different clusters of sections (Figure 5A and see Supplementary material online, Figure S4 and data file S3). Based on their epicardial location (Figure 3B) and marker gene expression indicating a high abundance of adipocytes (Figures 4A and B and 5B, and see Supplementary material online, Figure S5A and B), we concluded the Cluster 1 sections to represent the fibro-fatty region. Since Cluster 3 sections showed an enriched expression of cardiomyocyte markers (Figures 4E and F and 5C, see Supplementary material online, Figures S4B and S5C and D), we concluded those sections to represent the myocardial areas.

As Cluster 2 sections appeared to be located at the transition site between the fibro-fatty epicardial region and the myocardial region and interspersed within the myocardial area, we were wondering whether these sections were representing the gene expression profile of sites of active remodelling. Comparative gene analysis between the Cluster 2 and myocardial (Cluster 3) sections revealed 148 genes to be significantly enriched in the Cluster 2 sections, whereas 186 genes were significantly less abundant compared with the myocardial sections ( $P < 0.01$ ; Figure 5A). We noticed that the expression of several cardiomyocyte markers, such as *DES*, and Muscle creatine kinase (*CKM*) was reduced in the Cluster 3 sections vs. the Cluster 2 sections (Figure 5A). Furthermore, we observed an enrichment for adipocyte marker genes like *PLIN1*, and *ADH1B* in the Cluster 2 sections vs. the myocardial sections (Figure 5A). This was confirmed when visualizing the local abundance of transcript counts per gene, where we observed the lower abundance for *DES*, *MYH7*, and *CKM* (Figure 5C, and see Supplementary material online, Figure S5C and D) and enrichment for *PLIN1*, *ADH1B*, and *PLIN4* in a subset of Cluster 2 sections compared with the myocardial sections (Figure 5B and see Supplementary

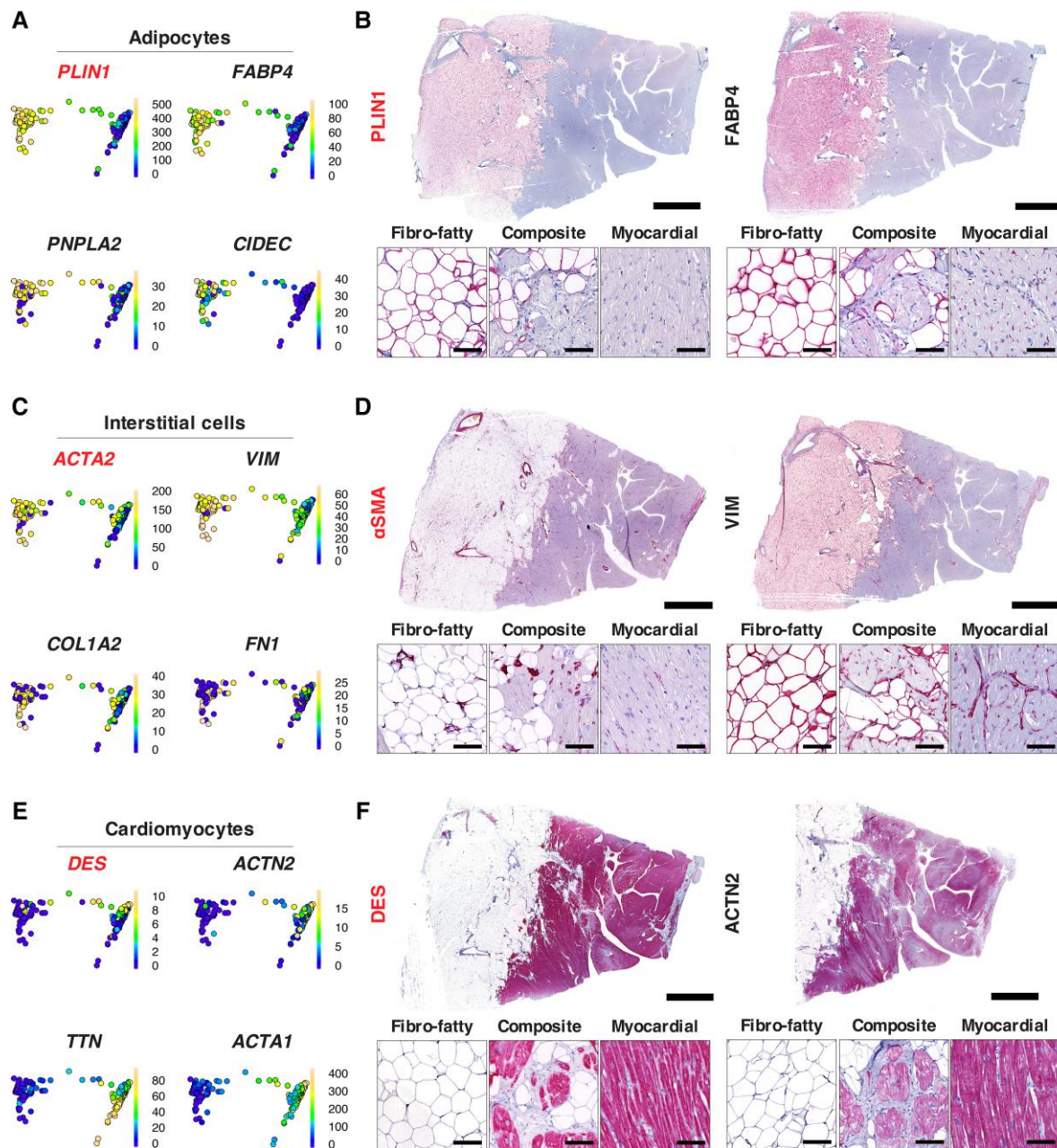


**Figure 4** Identification of region-specific gene expression in the ACM heart. PCA maps indicating the expression of four cellular markers in cell populations identified as adipocytes (A), interstitial cells (C), and cardiomyocytes (E). Each dot represents one section, colour-coded for normalized transcript counts from blue to yellow (low-to-high). Validation of protein expression pattern of two cellular markers including the reference marker (in red, left panel) in cell populations identified as adipocytes (B), interstitial cells (D), and cardiomyocytes (F) by immunostaining across the ACM heart. Scale bars 5 mm (overview) and 100  $\mu$ m (zoom panels).

material online, Figure S5A and B). Based on these findings, we concluded the Cluster 2 sections to represent the composite areas where the myocardial cells were actively being replaced by fibro-fatty cells. However, many sections of the composite region did not express adipocyte marker genes, indicating that the composite region is not merely a combination of myocyte and adipocyte cell types.

Interestingly, pathway analysis on the differentially expressed genes in the composite sections compared with the myocardial sections indicated the regulated genes to be functionally linked to apoptosis, metabolic

changes, and myocyte (dis)assembly (Figure 5D, Supplementary material online, data file S4). Since myocyte degeneration and fibro-fatty replacement of myocardial tissue are key hallmarks of disease progression during ACM, we hypothesized that genes activated in these regions might be actively contributing to the disease process.

Based on these observations, we searched for genes that were specifically induced in the composite sections compared with both myocardial and adipogenic sections, to function as local regulators of active remodelling. Based on these data, we identified Zinc finger and BTB domain-



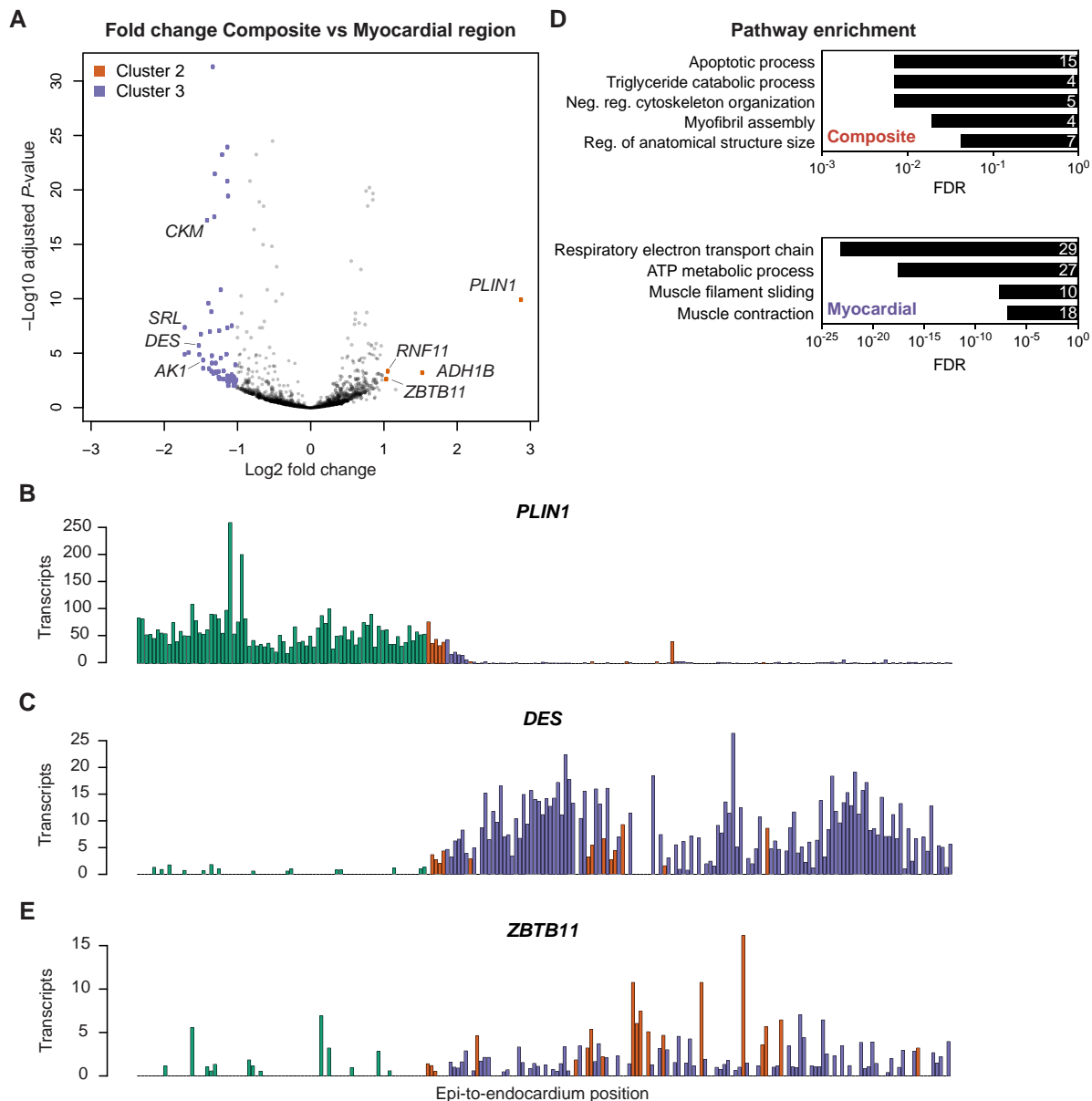


**Figure 5** Composite sections show enrichment for genes involved in apoptosis and cytoskeleton disorganization. (A) Differential gene expression analysis between the composite (Cluster 2) and myocardial region (Cluster 3). Each grey dot is a gene; colour-coded dots respective of each region indicate significant ( $P < 0.01$ ), at least two-fold enriched genes. (B) Expression profiles of the adipocyte marker *PLIN1*, (C) the cardiomyocyte marker *DES*, and (E) the composite region-enriched gene, *ZBTB11*. (D) Functional annotation of genes enriched in the composite region indicating increased cardiomyocyte apoptosis and negative regulation of cytoskeleton organization. The number of enriched genes per pathway is displayed at the right. FDR, false discovery rate.

containing protein 11 (*ZBTB11*), an ill-studied transcription factor, to be specifically induced in the composite sections (Figure 5A), which was confirmed when looking at the transcript counts of *ZBTB11* per individual section (Figure 5E).

To examine whether these cluster-specific gene programmes are a general feature of ACM, we next performed Tomo-Seq on an additional male heart with a mutation in the desmoplakin gene (*DSP* [NM\_004415.4]; p.Lys569X) (Supplementary material online, data file S5). This heart displayed typical histological features of ACM, such as fibro-fatty replacement tissue at the epicardial side, composite region, and myocardium (see Supplementary material online, Figure S6A). The mutation led to a

reduction in DSP protein levels, as well as PKG levels, while PKP2 and NCAD levels were not reduced compared with NF control hearts (see Supplementary material online, Figure S1C and D). Pairwise comparison of sections across all expressed genes revealed a similar spatial partitioning (see Supplementary material online, Figure S6B and data file S6).

Hierarchical clustering of sections revealed the presence of four distinct clusters. Sections in Cluster 0 at the far epicardial and endocardial sides were excluded from further analysis (see Supplementary material online, Methods). We identified an epicardial-enriched Cluster 1, marked by high *PLIN1* expression, a myocardial cluster marked by *DES* expression (Cluster 3), and sections intermingled with myocardial

sections (Cluster 2; see [Supplementary material online, Figure S6C–F](#)). In line with our findings in the PKP2 mutant heart, functional annotation of differentially expressed genes between the composite sections and myocardial region (see [Supplementary material online, Figure S7A](#) and [data file S7](#)) revealed enrichment for metabolism and autophagy-related genes in the composite region, while cardiac muscle contraction and calcium signalling were negatively regulated (see [Supplementary material online, Figure S7B](#) and [data file S8](#)). Next, we plotted the expression profiles of key genes per section and noted that *PLIN1* was enriched in and adjacent to the epicardial fibro-fatty section (see [Supplementary material online, Figure S7C](#), Cluster 1, green). *DES* was most abundantly expressed in the myocardial sections (see [Supplementary material online, Figure S7C](#), Cluster 3, purple). Notably, Cluster 2 sections appeared enriched for *ZBTB11* expression, while showing a low *DES* expression (see [Supplementary material online, Figure S7C](#), orange).

These data indicate that processes related to cardiomyocyte degeneration are activated in the composite sections from ACM hearts and that this corresponds to enhanced *ZBTB11* expression.

### 3.7 ZBTB11 is induced in cardiomyocytes adjacent to fibro-fatty areas

Under homeostatic conditions, *ZBTB11* is only expressed at low levels in the heart compared to other organs (see [Supplementary material online, Figure S8A](#)). Using western blot analysis, we were able to confirm elevated *ZBTB11* protein levels in LV tissue from the PKP2 and DSP mutant hearts used for the Tomo-Seq experiments (see [Supplementary material online, Figure S8B](#)). To determine the cardiac cell type responsible for the induction in *ZBTB11* expression, we performed IHC on ACM hearts. This indicated *ZBTB11* protein to be enriched in cardiomyocytes that are flanked by fibro-fatty patches ([Figure 6A](#), and see [Supplementary material online, Figure S8C](#)). In counterstaining these sections with *DES*, a gene shown to be decreased in the composite sections compared with the myocardial sections ([Figure 5A](#)), we noticed a marked loss of *DES* in the *ZBTB11*-positive cardiomyocytes ([Figure 6A](#)). The enrichment for *ZBTB11* in cardiomyocytes flanked by fibro-fatty regions could be confirmed in three additional hearts of ACM patients with a *PKP2* mutation ([Figure 6B](#)). As fibro-fatty replacement is also seen in other genetic cardiomyopathies, we analysed *ZBTB11* expression in hearts explanted from non-*PKP2* or -*DSP* mutation carriers and observed a similar increase in *ZBTB11* in cardiomyocytes neighbouring fibro-fatty areas ([Figure 6C](#)). Fatty infiltrations can also be observed in ischaemic heart failure near old infarcts. We assessed *ZBTB11* expression and found that cardiomyocytes near fatty infiltrates also display enhanced *ZBTB11* staining (see [Supplementary material online, Figure S8D](#)). To rule out that *ZBTB11* is part of a conserved generic cell death-associated pathway in the heart, we analysed *ZBTB11* expression in multiple mouse models of heart disease without fibro-fatty infiltrations and found no evidence for such a function (see [Supplementary material online, Figure S8E](#)). Together, these data imply that the upregulation of *ZBTB11* in diseased cardiomyocytes requires external stimuli, likely including the presence of fibro-fatty tissue.

### 3.8 ZBTB11 induces cardiomyocyte autophagy and apoptosis in cardiomyocytes

As *ZBTB11* induction in cardiomyocytes contiguous to fibro-fatty tissue appeared to be a consistent feature of cardiomyopathies, we aimed to

further explore the biological consequences of enhanced *ZBTB11* expression in human cardiomyocytes. To explore processes regulated by *ZBTB11* at these loci of myocardial disintegration, we analysed the genes that were most tightly co-expressed with *ZBTB11* in the human PKP2 ACM heart. The best correlated genes to *ZBTB11* included the autophagy and apoptosis-related gene Sequestosome 1 (*SQSTM1*, encoding P62); *RAB18*, a gene involved in lipid droplets' ER localization; and Vesicle trafficking (CLTC, Clathrin) and loading (*SYNCRIP*) related genes (see [Supplementary material online, Figure S9A](#) and [data file S2](#)). Gene ontology and KEGG pathway analysis of the top 25 correlated genes further revealed enrichment for pathways involved in vesicle-mediated transport and chaperone-mediated autophagy (see [Supplementary material online, Figure S9B and C](#) and [data file S9](#)). To establish whether autophagy was enhanced in human ACM hearts, we performed western blot analysis for P62 in the PKP2 and DSP mutant hearts and found that P62 levels were elevated in the ACM hearts compared with NF control hearts (see [Supplementary material online, Figure S9D and E](#)). These results suggest that *ZBTB11* expression is associated with autophagy and apoptosis, in line with our observations that *ZBTB11* expression is specifically enhanced at loci of myocardial disintegration ([Figures 5D and 6](#)).

To study the direct functional effect of *ZBTB11*, we infected iPS-derived cardiomyocytes (iPS-CM) with a virus overexpressing human *ZBTB11* (AAV6-*ZBTB11*) or a control virus (AAV6-GFP; [Figure 7A](#) and see [Supplementary material online, Figure S10A and B](#)). While *ZBTB11* localized preferentially to the nuclei of transduced cells, it was also detected in the cytoplasm in a subset of cells (see [Supplementary material online, Figure S11D and E](#)), and was barely detectable in cells transduced with control virus ([Figure 7B](#), and see [Supplementary material online, Figure S10C](#)). *ZBTB11* transduced cardiomyocytes appeared morphologically normal and FACS indicated comparable numbers of cardiomyocytes for both groups (see [Supplementary material online, Figure S10D and E](#)).

RNA sequencing indicated that *ZBTB11* overexpression resulted in marked gene expression changes ([Figure 7C](#)), with 80 genes over- and 50 genes underexpressed compared with control cardiomyocytes (fold change 1.5×, adjusted *P*-value <0.05) ([Figure 7D](#)). Amongst the upregulated genes and in line with the Tomo-Seq data, there was a striking enrichment of genes related to the P53 pathway, apoptosis, and autophagy ([Figure 7E](#) and [Supplementary material online, data file S10](#)). Furthermore, *ZBTB11* overexpression was associated with decreased expression of genes driving translational regulation and cardiomyocyte contraction. The P53 pathway is a stress response pathway that is activated by post-translational modifications to the P53 protein and initiates a programme of cell cycle arrest, cellular senescence, or apoptosis.<sup>18</sup> We found that *P53* expression both at the mRNA and the protein level was not significantly altered by *ZBTB11* overexpression ([Figure 7F–H](#), see [Supplementary material online, Figure S10G and H](#)). However, P53 target genes driving apoptosis, such as Growth arrest and DNA damage-inducible protein 45 (*GADD45A*), Fas cell surface death receptor (*FAS*), and Tumour necrosis factor receptor superfamily member 21 (*TNFRSF21*) were markedly upregulated, as were key regulators of autophagy and lysosomal acidification Tripartite motif-containing 22 (*TRIM22*), Polo-like kinase 2 (*PLK2*), ATPase, and H<sup>+</sup> transporting V1 subunit G2 (*ATP6V1G2*) ([Figure 7F](#)).

As overexpression of *ZBTB11* led to a marked decrease in cardiomyocyte contraction genes and we observed an inverse correlation between *ZBTB11* and *DES* expression in the composite region in the ACM heart ([Figure 6A](#)), we decided to further examine *DES* expression in our iPS-CM model. *ZBTB11* overexpression induced a significant downregulation of *DES* at the protein level ([Figure 7G and H](#)), while

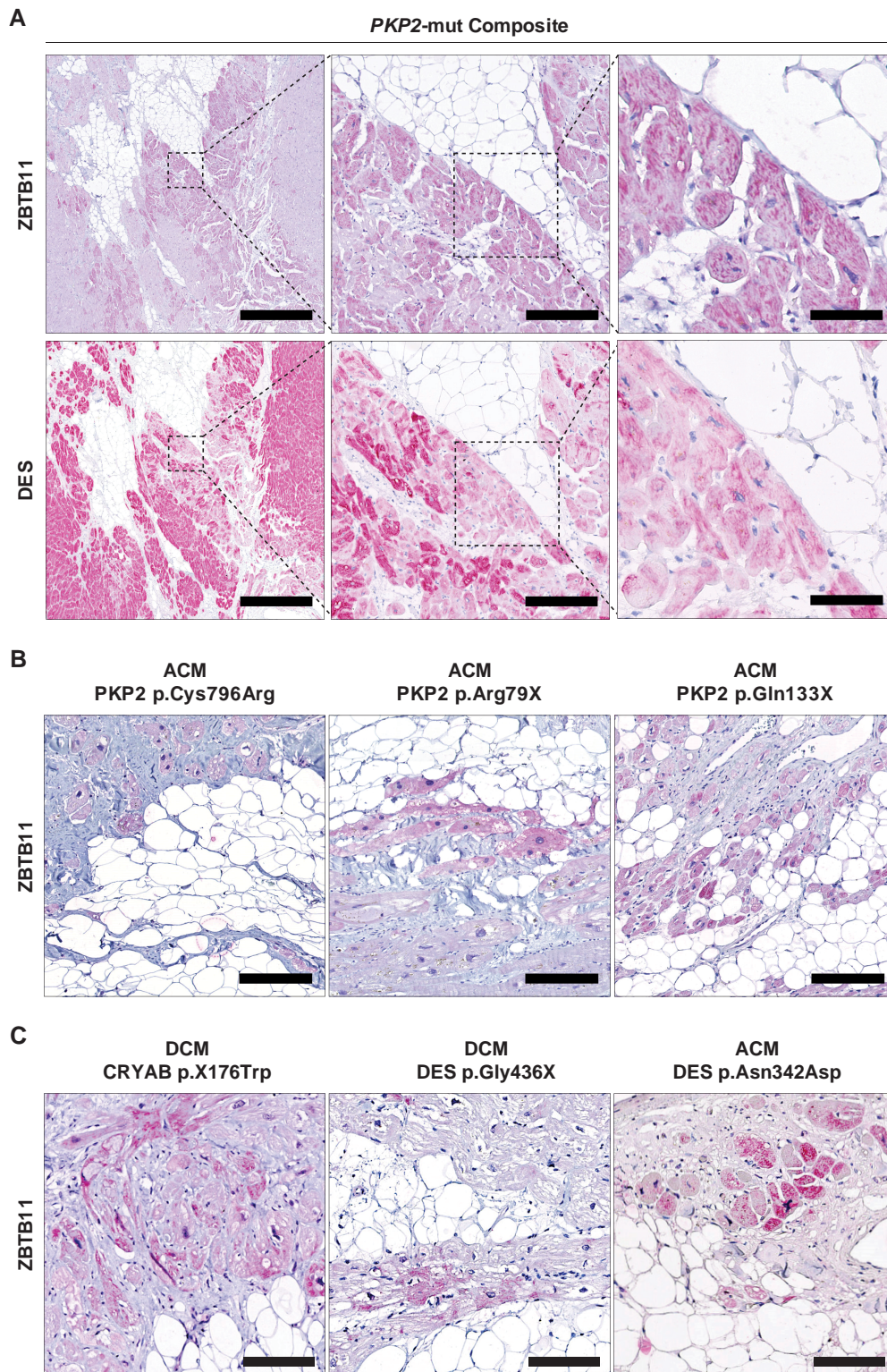


**Figure 6** ZBTB11 marks cardiomyocytes surrounded by fibro-fatty replacement. (A) ZBTB11 immunostaining reveals positive cardiomyocytes in the composite region in the ACM heart, which is paralleled with a loss in DES. Scale bars, 800  $\mu$ m (left); 150  $\mu$ m (middle); 75  $\mu$ m (right). (B) Enrichment of ZBTB11 in cardiomyocytes flanking fibro-fatty areas is also observed in additional ACM hearts harbouring different PKP2 mutations. (C) ZBTB11 immunostaining shows a similar enrichment in other genetic cardiomyopathic hearts. Scale bars in B and C, 100  $\mu$ m.

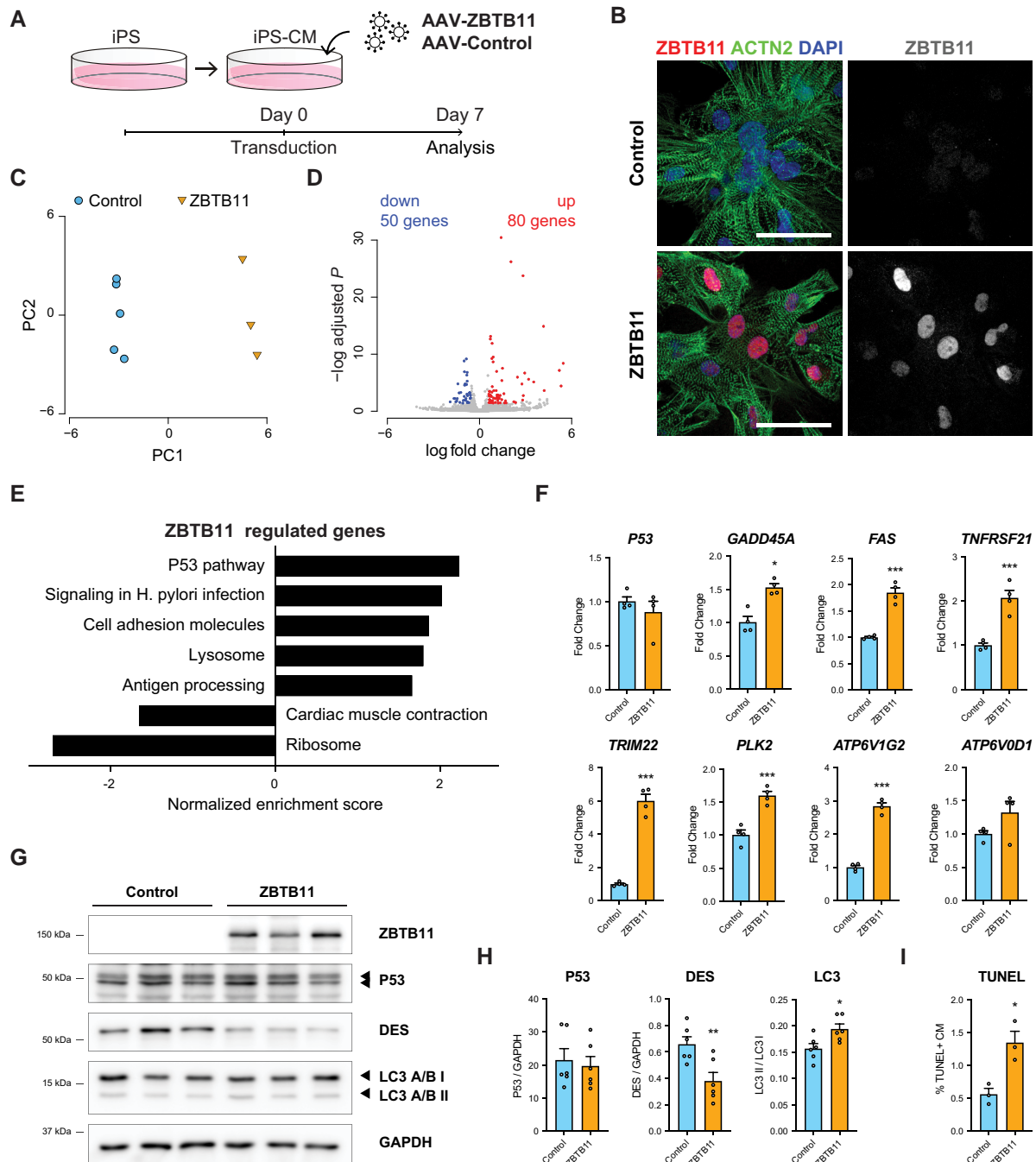


**Figure 7** ZBTB11 overexpression in iPS-CM induces autophagy and apoptosis. (A) Human iPS-CM were transduced with AAV-ZBTB11 or control virus. (B) ZBTB11 and ACTN2 immunostaining in iPS-CM 7 days after transduction. (C) PCA of RNA-Seq results. (D) Volcano plot of Log<sub>2</sub> fold change vs. Log<sub>10</sub> adjusted *P* showing regulated genes after ZBTB11 overexpression vs. control. (E) GSEA revealing pathways enriched and suppressed after ZBTB11 overexpression. (F) qRT-PCR for genes involved in apoptosis and autophagy. *n* = 4; multiplicity-adjusted *P*-values from the Holm–Sidak method after Student’s *t*-test. (G) Western blot and quantification (H) of iPS-CM after ZBTB11 overexpression. *n* = 6; two-tailed Student’s *t*-test. (I) Quantification of TUNEL-positive cardiomyocyte nuclei over total cardiomyocyte nuclei. *n* = 3; two-tailed Student’s *t*-test. \**P* < 0.05; \*\**P* < 0.01; \*\*\**P* < 0.001. Scale bar in B 50  $\mu$ m.

this was not observed at the mRNA level (*P* = 0.1377, Student’s *t*-test; see [Supplementary material online, Figure S10F](#)).

Autophagy is an adaptive cellular stress response that promotes cell death. The initiation of autophagy induces the conversion of cytosolic microtubule-associated protein 1 light chain 3 (LC3-I) to LC3-II, thereby

facilitating LC3-II incorporation into autophagosome membranes. The LC3-II/LC3-I ratio is therefore indicative of the amount of ongoing autophagy.<sup>19</sup> Western blot analysis confirmed an increase in the LC3-II/LC3-I ratio in ZBTB11 transduced cells, suggesting enhanced autophagy after ZBTB11 overexpression (Figure 7G and H). This effect was

further enhanced by the late-phase autophagy inhibitor Bafilomycin, which also exacerbated ZBTB11-induced accumulation of the autophagic cargo receptor P62 (see [Supplementary material online, Figure S10I](#)). Using terminal deoxynucleotidyl transferase dUTP nick end labelling (TUNEL) to label double-strand DNA breaks typical of apoptotic DNA fragmentation, we could also show ZBTB11 overexpression to significantly increase the fraction of apoptotic cardiomyocytes ([Figure 7I](#), see [Supplementary material online, Figure S10J](#)), confirming that ZBTB11 overexpression induces apoptosis in human cardiomyocytes. Next, we used hypoxic stress as a means to accentuate these effects of ZBTB11 in a cellular setting that is more similar to diseased hearts. Hypoxic stress substantially induced apoptosis and autophagy in iPS-CM, which was further enhanced by ZBTB11 overexpression (see [Supplementary material online, Figure S11A–C](#)). Moreover, when assessing the cellular localization of ZBTB11, we observed increased cytoplasmic localization of ZBTB11 under hypoxic stress conditions (see [Supplementary material online, Figure S11D and E](#)).

Together, the combined results from human ACM hearts and experiments in human cardiomyocytes indicate that ZBTB11 is increased in stressed cardiomyocytes flanking fibro-fatty regions in patients and that it induces autophagy and apoptosis in cardiomyocytes. These findings are compatible with the hypothesis that ZBTB11 in cardiomyocytes contributes to cardiomyocyte degeneration during genetic cardiomyopathy.

## 4. Discussion

Myocardial replacement by fibrous and fatty tissue due to cumulative myocyte loss by either apoptosis or necrosis is a key pathological hallmark of ACM.<sup>8</sup> While seminal studies using patient material and mouse models have identified key pathways, such as Wnt signalling<sup>20–23</sup> the Hippo pathway,<sup>24,25</sup> and changes in calcium handling<sup>26,27</sup> to be relevant for the disease, still many aspects of ACM remodelling remain undefined. Here, we used Tomo-Seq to generate a genome-wide gene expression atlas of human ACM hearts with high spatial resolution. This resource could be utilized to link local remodelling responses to changes in gene expression and identify new genes and pathways relevant for the disease. While Tomo-Seq already proved its value for revealing novel genes and pathways in animal models of heart disease,<sup>10,11</sup> this is the first time this technology is being used on human hearts to define disease-driving mechanisms in genetic cardiomyopathy.

Using Tomo-Seq on explanted ACM hearts, we were able to identify gene expression profiles at sites where degenerating cardiomyocytes are flanked by fibrous and fatty cells and where active remodelling is taking place.

Amongst genes marking the composite regions of myocardium, we identified ZBTB11 to be specifically enriched in cardiomyocytes present in this area. ZBTB proteins are characterized by having one or more C-terminal C<sub>2</sub>H<sub>2</sub>/Krüppel-type zinc finger (ZF) domains and an N-terminal BTB (broad-complex, tram-track, and bric-a-brac) domain and form an evolutionarily conserved family of transcription factors.<sup>28</sup> The BTB domain directly interacts with different corepressors and histone/protein modification enzymes, including NCOR-1/2 (nuclear receptor corepressor-1/2), BCOR (BCL6 corepressor), CTBP1, SIN3A, HDAC, and CUL3, and thus mediates chromatin remodelling and gene silencing/activation.<sup>29,30</sup> In contrast, the ZF domains determine the transcriptional specificity of ZBTB proteins through binding to regulatory regions in targeted genes in a sequence-specific manner.<sup>31</sup> While little is known about ZBTB11, functionally it was linked to neutrophil

development in zebrafish.<sup>32</sup> In line with the observation that inflammatory signalling is activated in ACM, ZBTB11 could also have a role in neutrophil development in the context of ACM disease progression.<sup>32,33</sup> Although that study showed P53 to be a direct downstream target of ZBTB11, we were unable to confirm this in cardiomyocytes. Nonetheless, our data clearly show that ZBTB11 has a role in cardiomyocyte degeneration, as increasing the level of ZBTB11 resulted in an elevated expression of genes related to autophagy and apoptosis and an increase in cardiomyocyte loss.

This role for ZBTB11 is especially interesting as cardiomyocyte loss is a characteristic feature of ACM, resulting in the loss of cardiac muscle and wall thinning. Several studies have shown the presence of apoptotic cells in ACM patient samples and that programmed cell death is likely the cause of cardiomyocyte loss.<sup>34–36</sup>

While the loss of contractile tissue contributes to a decline in function, extensive, patchy cardiomyocyte loss and fibro-fatty infiltration also create a myocardial substrate that is highly vulnerable to arrhythmia.<sup>37</sup> Blocking myocardial degeneration could therefore be a great benefit to patients suffering from genetic cardiomyopathy. Recent studies in mouse models of ACM have exposed pathways that may be involved in driving cardiomyocyte loss, such as activation of Ca<sup>2+</sup>-dependent cysteine proteases and epicardium-derived paracrine factors.<sup>38,39</sup> Although our data indicate ZBTB11 to induce cardiomyocyte loss, future experiments will have to show whether therapeutic inhibition of ZBTB11 can salvage viable myocardium during heart disease.

The specific expression of ZBTB11 in composite regions suggests that ZBTB11 is induced in response to fibro-fatty tissue. Mechanistically, this could involve changes in mechanical signals such as extracellular force,<sup>40,41</sup> cell–cell contacts, or other molecular signalling pathways.<sup>42,43</sup> ACM-associated fibro-fatty replacement is often associated with inflammatory cell infiltrates, which in turn can induce oxidative stress.<sup>44,45</sup> Hypoxia is a known inducer of apoptosis in cardiomyocytes,<sup>46</sup> and may also be involved in the regulation of ZBTB11. However, our findings in mouse ischaemic heart disease models suggest that hypoxia does not seem to be sufficient to drive ZBTB11 expression in cardiomyocytes. Moreover, while being known as a transcription factor, ZBTB11 was also abundantly detected in the cytoplasm in composite region cardiomyocytes. While the functional relevance of cytoplasmic localization is as yet unknown, we noticed that applying additional hypoxic stress exacerbated cytoplasmic ZBTB11 levels in transduced iPS-CM. It is conceivable that re-localization of ZBTB11 to the cytoplasm is a consequence of hypoxic stress. Further studies are required to reveal the exact regulatory mechanism underlying ZBTB11 induction and localization.

Our human *in vivo* and *in vitro* data show that an increase in ZBTB11 corresponds to a decrease in DES, an intermediate filament expressed in cardiomyocytes and other muscle cells. DES integrates the sarcolemma, Z-disk, and nuclear membrane in sarcomeres to regulate sarcomere structure and function.<sup>47</sup> Human DES mutations can lead to a loss in normal protein function or gain in toxic function and have been linked to mitochondrial defects and cardiomyocyte death.<sup>48</sup> It is currently unclear whether the loss of DES is a direct consequence of the increase in ZBTB11 or whether this is secondary to cells undergoing apoptosis. However, if ZBTB11 is indeed capable of regulating DES at the protein level, this could have far-reaching implications as DES loss of function mutations are associated with skeletal myopathies, DCM, and ACM.<sup>15,49</sup>

Currently, patients with genetic cardiomyopathies are still receiving generic heart failure drugs, intending to prevent life-threatening arrhythmias and progressive heart failure. However, with current technological

advancements in medical research, there are incredible opportunities to develop better-suited therapies. New developments in sequencing, genome editing, and iPS technologies are currently providing unprecedented possibilities to obtain new insights into disease-driving mechanisms underlying cardiac indications. Improving our understanding of the fundamental mechanisms that drive the pathological features of heart disease provides opportunities to develop better-targeted therapeutics. Here, we combined Tomo-Seq with IHC and studies in iPSC-derived cardiomyocytes to define relevant players during cardiac remodelling in ACM and identified ZBTB11 as an important inducer of cardiomyocyte apoptosis. Due to the importance of cardiac inflammation during ACM, ZBTB11 might additionally play a role there, which warrants further investigation. Follow-up studies will serve to define whether the inhibition of ZBTB11 is therapeutically beneficial in the setting of genetic cardiomyopathy.

## Supplementary material

Supplementary material is available at *Cardiovascular Research* online.

## Authors' contributions

C.J.B., G.P.A.L., Ab.V., A.B., and E.v.R.: conceptualization; C.J.B., G.P.A.L., A.B., S.J.v.K., I.P., H.d.R., D.V., P.v.d.K., M.G., N.d.J., J.P.J., and Ar.V.: methodology; C.J.B., G.P.A.L., Ab.V.: investigation; Ab.V.: analysis and visualization Tomo-Seq data; C.J.B., E.v.R., and A.v.O.: funding acquisition; E.v.R., A.v.O., and Ar.V.: supervision; C.J.B., G.P.A.L., Ab.V., and E.v.R.: writing—original draft; S.J.v.K., I.P., H.d.R., D.V., A.B., P.v.d.K., M.G., N.d.J., J.P.J., A.v.O., and Ar.V.: writing—review and editing.

## Acknowledgements

We thank Erica Siera-de Koning for assistance with obtaining human explant heart material for Tomo-Seq experiments. We thank Utrecht Sequencing Facility for providing sequencing service and data. Utrecht Sequencing Facility is subsidized by the University Medical Center Utrecht, Hubrecht Institute, Utrecht University, and The Netherlands X-omics Initiative (NWO project 184.034.019).

**Conflict of interest:** None declared.

## Funding

This work was supported by the Leducq Foundation (grant 14CVD04 to E.v.R.); the European Research Council under the European Union's Seventh Framework Program (grant agreement CoG 615708 MICARUS to E.v.R.); the Dutch Cardiovascular Alliance, an initiative with support of the Dutch Heart Foundation (DCVA2017-18 CVON-PRIME to E.v.R.); and the European Union's Horizon 2020 research and innovation program (Marie Skłodowska-Curie grant agreement no. 751988 to C.J.B.).

## Data availability

RNA-Seq data are deposited at NCBI Gene Expression Omnibus repository, accession number GSE114770, and analysis scripts are available under <https://github.com/vertesy/ACM.Tomo-Seq>.

## References

- Dalal D, Molin LH, Piccini J, Tichnell C, James C, Bomma C, Prakasa K, Towbin JA, Marcus FI, Spevak PJ, Bluemke DA, Abraham T, Russell SD, Calkins H, Judge DP. Clinical features of arrhythmogenic right ventricular dysplasia/cardiomyopathy associated with mutations in plakophilin-2. *Circulation* 2006;**113**:1641–1649.
- Finocchiaro G, Papadakis M, Robertus JL, Dhutia H, Steriotis AK, Tome M, Mellor G, Merghani A, Malhotra A, Behr E, Sharma S, Sheppard MN. Etiology of sudden death in sports: insights from a United Kingdom regional registry. *J Am Coll Cardiol* 2016;**67**:2108–2115.
- Marian AJ, van Rooij E, Roberts R. Genetics and genomics of single-gene cardiovascular diseases: common hereditary cardiomyopathies as prototypes of single-gene disorders. *J Am Coll Cardiol* 2016;**68**:2831–2849.
- Vermij SH, Abriel H, van Veen TA. Refining the molecular organization of the cardiac intercalated disc. *Cardiovasc Res* 2017;**113**:259–275.
- Bhonsale A, Groeneweg JA, James CA, Dooijes D, Tichnell C, Jongbloed JD, Murray B, te Riele AS, van den Berg MP, Bikker H, Atsma DE, de Groot NM, Houweling AC, van der Heijden JF, Russell SD, Doevendans PA, van Veen TA, Tandri H, Wilde AA, Judge DP, van Tintelen JP, Calkins H, Hauer RN. Impact of genotype on clinical course in arrhythmogenic right ventricular dysplasia/cardiomyopathy-associated mutation carriers. *Eur Heart J* 2015;**36**:847–855.
- Gerull B, Heuser A, Wichter T, Paul M, Basson CT, McDermott DA, Lerman BB, Markowitz SM, Ellinor PT, MacRae CA, Peters S, Grossmann KS, Drenckhahn J, Michely B, Sasse-Klaassen S, Birchmeier W, Dietz R, Breithardt G, Schulze-Bahr E, Thierfelder L. Mutations in the desmosomal protein plakophilin-2 are common in arrhythmogenic right ventricular cardiomyopathy. *Nat Genet* 2004;**36**:1162–1164.
- James CA, Calkins H. Arrhythmogenic right ventricular cardiomyopathy: progress toward personalized management. *Annu Rev Med* 2019;**70**:1–18.
- Hoorntje ET, Te Rijdt WP, James CA, Pilichou K, Basso C, Judge DP, Bezzina CR, van Tintelen JP. Arrhythmogenic cardiomyopathy: pathology, genetics, and concepts in pathogenesis. *Cardiovasc Res* 2017;**113**:1521–1531.
- Junker JP, Noel ES, Guryev V, Peterson KA, Shah G, Huiskens J, McMahon AP, Berezikov E, Bakkers J, van Oudenaarden A. Genome-wide RNA tomography in the zebrafish embryo. *Cell* 2014;**159**:662–675.
- Wu CC, Kruse F, Vasudevarao MD, Junker JP, Zebrowski DC, Fischer K, Noel ES, Grun D, Berezikov E, Engel FB, van Oudenaarden A, Weidinger G, Bakkers J. Spatially resolved genome-wide transcriptional profiling identifies bmp signaling as essential regulator of zebrafish cardiomyocyte regeneration. *Dev Cell* 2016;**36**:36–49.
- Lacruz GPA, Junker JP, Gladka MM, Molenaar B, Scholman KT, Vigil-Garcia M, Versteeg D, de Ruiter H, Vermunt MW, Creighton MP, Huibers MMH, de Jonge N, van Oudenaarden A, van Rooij E. Tomo-Seq identifies SOX9 as a key regulator of cardiac fibrosis during ischemic injury. *Circulation* 2017;**136**:1396–1409.
- van Tintelen JP, Entius MM, Bhuiyan ZA, Jongbloed R, Wiesfeld AC, Wilde AA, van der Smagt J, Boven LG, Mannens MM, van Langen IM, Hofstra RM, Otterspoor LC, Doevendans PA, Rodriguez LM, van Gelder IC, Hauer RN. Plakophilin-2 mutations are the major determinant of familial arrhythmogenic right ventricular dysplasia/cardiomyopathy. *Circulation* 2006;**113**:1650–1658.
- Burridge PW, Holmstrom A, Wu JC. Chemically defined culture and cardiomyocyte differentiation of human pluripotent stem cells. *Curr Protoc Hum Genet* 2015;**87**:21.3.1–21.3.15.
- Love MI, Huber W, Anders S. Moderated estimation of fold change and dispersion for RNA-seq data with DESeq2. *Genome Biol* 2014;**15**:550.
- Bermudez-Jimenez FJ, Carriel V, Brodehl A, Alaminos M, Campos A, Schirmer I, Milting H, Abril BA, Alvarez M, Lopez-Fernandez S, Garcia-Giustinianni D, Monserrat L, Tercedor L, Jimenez-Jaimez J. Novel desmin mutation p.Glu401Asp impairs filament formation, disrupts cell membrane integrity, and causes severe arrhythmogenic left ventricular cardiomyopathy/dysplasia. *Circulation* 2018;**137**:1595–1610.
- Delmar M, McKenna WJ. The cardiac desmosome and arrhythmogenic cardiomyopathies: from gene to disease. *Circ Res* 2010;**107**:700–714.
- Rohr S. Molecular crosstalk between mechanical and electrical junctions at the intercalated disc. *Circ Res* 2007;**101**:637–639.
- Morita H, Komuro I. Heart failure as an aging-related phenotype. *Int Heart J* 2018;**59**:6–13.
- Tanida I, Ueno T, Kominami E. LC3 and autophagy. *Methods Mol Biol* 2008;**445**:77–88.
- Asimaki A, Syrris P, Wichter T, Matthias P, Saffitz JE, McKenna WJ. A novel dominant mutation in plakoglobin causes arrhythmogenic right ventricular cardiomyopathy. *Am J Hum Genet* 2007;**81**:964–973.
- Garcia-Gras E, Lombardi R, Giocondo MJ, Willerson JT, Schneider MD, Khoury DS, Marian AJ. Suppression of canonical Wnt/beta-catenin signaling by nuclear plakoglobin recapitulates phenotype of arrhythmogenic right ventricular cardiomyopathy. *J Clin Invest* 2006;**116**:2012–2021.
- Li J, Swope D, Raess N, Cheng L, Muller EJ, Radice GL. Cardiac tissue-restricted deletion of plakoglobin results in progressive cardiomyopathy and activation of {beta}-catenin signaling. *Mol Cell Biol* 2011;**31**:1134–1144.
- Oxford EM, Danko CG, Fox PR, Kornreich BG, Moise NS. Change in beta-catenin localization suggests involvement of the canonical Wnt pathway in Boxer dogs with arrhythmogenic right ventricular cardiomyopathy. *J Vet Intern Med* 2014;**28**:92–101.
- Chen SN, Gurha P, Lombardi R, Ruggiero A, Willerson JT, Marian AJ. The hippo pathway is activated and is a causal mechanism for adipogenesis in arrhythmogenic cardiomyopathy. *Circ Res* 2014;**114**:454–468.
- Hu Y, Pu WT. Hippo activation in arrhythmogenic cardiomyopathy. *Circ Res* 2014;**114**:402–405.
- Cerrone M, Montnach J, Lin X, Zhao YT, Zhang M, Agullo-Pascual E, Leo-Macias A, Alvarado FJ, Dolgalev I, Karathanos TV, Malkani K, Van Opbergen CJM, van Bavel JJA,

- Yang HQ, Vasquez C, Tester D, Fowler S, Liang F, Rothenberg E, Heguy A, Morley GE, Coetzee WA, Trayanova NA, Ackerman MJ, van Veen TAB, Valdivia HH, Delmar M. Plakophilin-2 is required for transcription of genes that control calcium cycling and cardiac rhythm. *Nat Commun* 2017;**8**:106.
27. Kim JC, Perez-Hernandez M, Alvarado FJ, Maurya SR, Montnach J, Yin Y, Zhang M, Lin X, Vasquez C, Heguy A, Liang FX, Woo SH, Morley GE, Rothenberg E, Lundby A, Valdivia HH, Cerrone M, Delmar M. Disruption of Ca(2+) homeostasis and connexin 43 hemichannel function in the right ventricle precedes overt arrhythmogenic cardiomyopathy in plakophilin-2-deficient mice. *Circulation* 2019;**140**:1015–1030.
28. Zhu C, Chen G, Zhao Y, Gao XM, Wang J. Regulation of the development and function of B cells by ZBTB transcription factors. *Front Immunol* 2018;**9**:580.
29. Beaulieu AM, Sant'Angelo DB. The BTB-ZF family of transcription factors: key regulators of lineage commitment and effector function development in the immune system. *J Immunol* 2011;**187**:2841–2847.
30. Mathew R, Seiler MP, Scanlon ST, Mao AP, Constantinides MG, Bertozzi-Villa C, Singer JD, Bendelac A. BTB-ZF factors recruit the E3 ligase cullin 3 to regulate lymphoid effector programs. *Nature* 2012;**491**:618–621.
31. Maeda T. Regulation of hematopoietic development by ZBTB transcription factors. *Int J Hematol* 2016;**104**:310–323.
32. Keightley MC, Carradice DP, Layton JE, Pase L, Bertrand JY, Wittig JG, Dakic A, Badrock AP, Cole NJ, Traver D, Nutt SL, McCoe J, Buckle AM, Heath JK, Lieschke GJ. The Pu.1 target gene Zbtb11 regulates neutrophil development through its integrase-like HHCC zinc finger. *Nat Commun* 2017;**8**:14911.
33. Asatryan B, Asimaki A, Landstrom AP, Khanji MY, Odening KE, Cooper LT, Marchlinski FE, Gelzer AR, Semsarian C, Reichlin T, Owens AT, Chahal CAA. Inflammation and immune response in arrhythmogenic cardiomyopathy: state-of-the-art review. *Circulation* 2021;**144**:1646–1655.
34. Kavantzias NG, Lazaris AC, Agapitos EV, Nanas J, Davaris PS. Histological assessment of apoptotic cell death in cardiomyopathies. *Pathology* 2000;**32**:176–180.
35. Mallat Z, Tedgui A, Fontaliran F, Frank R, Durigon M, Fontaine G. Evidence of apoptosis in arrhythmogenic right ventricular dysplasia. *N Engl J Med* 1996;**335**:1190–1197.
36. Valente M, Calabrese F, Thiene G, Angelini A, Basso C, Nava A, Rossi L. In vivo evidence of apoptosis in arrhythmogenic right ventricular cardiomyopathy. *Am J Pathol* 1998;**152**:479–484.
37. De Coster T, Claus P, Kazbanov IV, Haemers P, Willems R, Sipido KR, Panfilov AV. Arrhythmogenicity of fibro-fatty infiltrations. *Sci Rep* 2018;**8**:2050.
38. Chelko SP, Keceli G, Carpi A, Doti N, Agrimi J, Asimaki A, Beti CB, Miyamoto M, Amat-Codina N, Bedja D, Wei AC, Murray B, Tichnell C, Kwon C, Calkins H, James CA, O'Rourke B, Halushka MK, Melloni E, Saffitz JE, Judge DP, Ruvo M, Kitsis RN, Andersen P, Di Lisa F, Paolocci N. Exercise triggers CAPN1-mediated AIF truncation, inducing myocyte cell death in arrhythmogenic cardiomyopathy. *Sci Transl Med* 2021;**13**.
39. Yuan P, Cheedipudi SM, Rouhi L, Fan S, Simon L, Zhao Z, Hong K, Gurha P, Marian AJ. Single cell RNA-sequencing uncovers paracrine functions of the epicardial-derived cells in arrhythmogenic cardiomyopathy. *Circulation* 2021;**143**:2169–2187.
40. Saucerman JJ, Tan PM, Buchholz KS, McCulloch AD, Omens JH. Mechanical regulation of gene expression in cardiac myocytes and fibroblasts. *Nat Rev Cardiol* 2019;**16**:361–378.
41. Hariharan V, Asimaki A, Michaelson JE, Plovie E, MacRae CA, Saffitz JE, Huang H. Arrhythmogenic right ventricular cardiomyopathy mutations alter shear response without changes in cell-cell adhesion. *Cardiovasc Res* 2014;**104**:280–289.
42. Austin KM, Trembley MA, Chandler SF, Sanders SP, Saffitz JE, Abrams DJ, Pu WT. Molecular mechanisms of arrhythmogenic cardiomyopathy. *Nat Rev Cardiol* 2019;**16**:519–537.
43. Antonopoulos AS, Antoniadou C. The role of epicardial adipose tissue in cardiac biology: classic concepts and emerging roles. *J Physiol* 2017;**595**:3907–3917.
44. Meraviglia V, Alcalde M, Campuzano O, Bellin M. Inflammation in the pathogenesis of arrhythmogenic cardiomyopathy: secondary event or active driver? *Front Cardiovasc Med* 2021;**8**:784715.
45. Garcia N, Zazueta C, Aguilera-Aguirre L. Oxidative stress and inflammation in cardiovascular disease. *Oxid Med Cell Longev* 2017;**2017**:5853238.
46. Giordano FJ. Oxygen, oxidative stress, hypoxia, and heart failure. *J Clin Invest* 2005;**115**:500–508.
47. Hnia K, Ramspacher C, Vermot J, Laporte J. Desmin in muscle and associated diseases: beyond the structural function. *Cell Tissue Res* 2015;**360**:591–608.
48. Capetanaki Y, Papatheanasiou S, Diokmetzidou A, Vatsellas G, Tsikitis M. Desmin related disease: a matter of cell survival failure. *Curr Opin Cell Biol* 2015;**32**:113–120.
49. Lorenzon A, Boffagna G, Bauce B, De Bortoli M, Li Mura IE, Calore M, Dazzo E, Basso C, Nava A, Thiene G, Rampazzo A. Desmin mutations and arrhythmogenic right ventricular cardiomyopathy. *Am J Cardiol* 2013;**111**:400–405.